



## Crack tip shielding effects, Part 1: direct measurement of the plastic enclave

E. A. Patterson

*School of Engineering, University of Liverpool (UK)*  
*eann.patterson@liverpool.ac.uk*

M. N. James

*Faculty of Science & Technology, University of Plymouth (UK)*

---

**ABSTRACT.** The direct observation or measurement of the size and shape of plastic zones associated with a propagating fatigue crack has been difficult. In earlier work the authors used the growth of fatigue cracks in polycarbonate specimens combined with transmission photoelasticity to observe qualitatively the plastic enclave ahead of a crack and the development of a plastic wake along the crack flanks. Recently this approach has been extended to studying the effect of overloads on the size of the plastic enclave and the correlation with crack growth rate. In more recent work thermoelastic stress analysis has been employed to map the size and shape of the plastic zone ahead of cracks in aluminum compact tension specimens. The phase difference between the measured temperature signal and the applied loading permitted the identification of the extent of plastic behavior, or the limit of thermoelastic behavior. Experiments were performed with overloads for single cycles and ten cycles and the change in size of the plastic enclave was defined and correlated to both stress intensity factor and growth rate. The coefficients in Wheeler's model were evaluated from direct measurements and used to reliably predict crack behavior. Work is in progress to obtain the strain field around the crack tip, both within and around the plastic zone using digital image correlation. The data from photoelasticity, thermoelastic stress analysis and digital image correlation confirm the influence on the crack growth rate of the plastic enclave associated with the crack tip and the plastic wake behind the tip. This influence occurs as a result of the plastic enclave shielding the crack tip from the full effect of the applied loading and the shear stresses established between the elastic and plastic regions in the wake. The traditional descriptions of the singularity-dominated, elastic stress field do not appear to be capable of describing this complex situation. The experimental data obtained with the above techniques has inspired the development of a new multi-parameter model in which the stress field can be characterized by a new set of intensity factors which quantify crack driving and crack retarding effects separately. As will be described in part II [1], the results from the new model correlate well with experimental measurements.

**KEYWORDS.** Thermoelasticity; Photoelasticity; Digital image correlation; Plastic enclave; Crack .

---

### INTRODUCTION

Crack closure [2] is a well-known but little-understood phenomenon [3]. The lack of understanding arises largely from the difficulties associated with making direct measurements related to any of the many possible driving mechanisms which include plasticity [2], flank roughness [4], oxides [5], viscous fluid [6] and phase-transformation

---



[7]. Originally, crack closure was described as occurring when crack faces contact prematurely during cyclic loading as a result of plasticity generated during crack growth and this leads to the term plasticity-induced closure. Thus, the focus of this work has been the use of techniques from experimental mechanics to identify and quantify the extent of the plastic enclave associated with a propagating fatigue crack. The motivation being initially to support the development of a new model of the forces associated with the role of the total plastic enclave during fatigue crack propagation; and then more recently to quantifying the extent of the enclave in order to validate various approaches to predicting fatigue behavior in the presence of plasticity-induced closure. Three techniques, i.e. photoelasticity, thermoelastic stress analysis and digital image correlation, were selected from experimental mechanics based on their ability to provide full-field maps of strain or stress around a propagating crack.

#### *Photoelasticity*

Photoelastic stress analysis is a classical technique of experimental stress analysis based on the temporary stress-induced birefringence of transparent materials, i.e. their ability to exhibit fringes related to the magnitude and direction of the principal stresses when viewed in polarised light [8]. In white light coloured interference fringes are observed and the number of fringes is linearly dependent on the difference in the principal strains in both elastic and plastic regions. In this work fatigue cracks were grown in thin sheets of polycarbonate which was used as a model of fatigue behaviour in other materials [9].

#### *Thermoelastic stress analysis (TSA)*

Thermoelasticity was observed and understood more than 150 years ago; however, its use as a means of evaluating stresses in engineering components only became viable about 30 years ago with advent of suitable instruments [10]. Nowadays a sensitive infra-red camera is used to monitor the very small changes in temperature induced in a material by changes in the stress or strain. When the elastic strain changes sufficiently fast to produce adiabatic conditions, then the measured changes in temperature are directly proportional to the change in the first strain invariant [11]. Heat generation as a consequence of contact or plastic deformation causes a phase shift in the measured temperature signal with respect to time [12].

#### *Digital Image Correlation*

Digital image correlation has become very popular in recent years due to the simplicity of its application and the level of information obtained. Digital images are taken before and after deformation of a component and the displacement of surface features contained within sub-images are tracked using a correlation algorithm [13]. It is usual to apply a speckle pattern to the surface of the component to enhance the ease and resolution of the analysis; however, it is possible to use the surface texture of the material for correlation purposes [14]. The use of a single camera provides in-plane deformation data while stereoscopic viewing with two cameras yields three-dimensional deformation data, i.e. in-plane and out-of-plane.

## **METHODS**

The data presented in Figs. 1 to 3 arise from three studies [15 – 17] conducted consecutively over the past decade at the Universities of Plymouth and Sheffield and at Michigan State University. The photoelastic image in Fig. 1 was obtained by viewing a compact tension specimen in a polarising microscope. The specimen was manufactured from 2mm thick polycarbonate sheet and otherwise followed ASTM E399 with overall dimensions of 90×67mm with a 38mm long starter notch. A fatigue crack was grown in the specimen using a cycle with a maximum load of 110N and an R-ratio of 0.1 at a frequency of 0.4Hz. When the crack had grown 20mm from the notch tip, the specimen was removed from the loading machine and examined in the microscope which was set up as a light field circular polariscope.

Fig. 2 shows the phase difference between the measured distribution of temperature and the applied loading in an aluminium compact tension specimen. The specimen was manufactured, based on ASTM E399, from aircraft grade aluminium alloy 2024-T3 to the same dimensions as the polycarbonate specimen. It was subjected to a cyclic load with a mean and amplitude of 1000N at a frequency of 10Hz. A focal plane array infra-red camera (DeltaTherm 1550, StressPhotonics Inc., Madison, WI) with a lock-in amplifier was utilised to acquire thermoelastic data continuously during fatigue crack growth. A reference signal from the loading machine was used to synchronise the temperature data in the elastic regions far from the crack tip with applied loading. Consequently, in Fig. 2 the phase values are largely zero (green)

except in two regions immediately adjacent to the crack. Ahead of the crack, an area of negative (blue) phase difference is found and along the crack flank there is an area of positive phase difference. A simple binary threshold was applied to the phase map in order to define the out-of-phase area ahead of the crack and the dimensions of this area are compared with Dugdale's [18] and Irwin's [19] expressions for the size of the crack tip plastic zone in Fig. 4.

The digital image correlation data shown in Fig. 3 was obtained using the same design of specimen as for the thermoelastic study except that aluminium had a yield strength of 345MPa and a modulus of 73GPa so that the yield strain was approximately  $4720\mu\epsilon$ . The specimen surface was sprayed with a very fine mist of black and then white paint so that bare metal was still visible and generated a very fine speckle pattern. The fatigue cycle consisted of a minimum load of 500N and a maximum load of 1500N applied at 10Hz, i.e. as for the thermoelastic data collection. Images were collected using a monochrome progressive scan 1/2" CCD camera with 1.4 Megapixels resolution (JAI, Glostrup, Denmark) fitted with an AF90mm F/2.8 Di 1:1 macro lens (Tamron, Commack, NY) and a PL-800 fiber optic illuminator (Dolan-Jenner Industries, Boxborough, MA) with a fiber optic ring light guide (2.37" inner diameter) to achieve the uniform illumination. The images of a 19×25mm area around the crack tip were processed using the Istra4D digital correlation software (Dantec Dynamics, Ulm, Germany) with  $61 \times 61$  pixel facets overlapped by 59 pixels to give displacement vectors at a pitch of 0.038mm. Strains were calculated from the displacement data using the standard algorithms in Istra4D software. The selection of the facet dimensions was critical because the facets needed to be large enough to permit accurate correlation without losing the detailed information about the deformation around the crack tip. The plastic zone was identified as those areas where the measured strain exceeded the material yield strain as shown in Fig. 3. The size of the plastic zone was defined as the maximum extent in the y-direction (perpendicular to the crack path) of the plastic region ahead of the crack and was plotted in Fig. 4 for comparison with the TSA data.

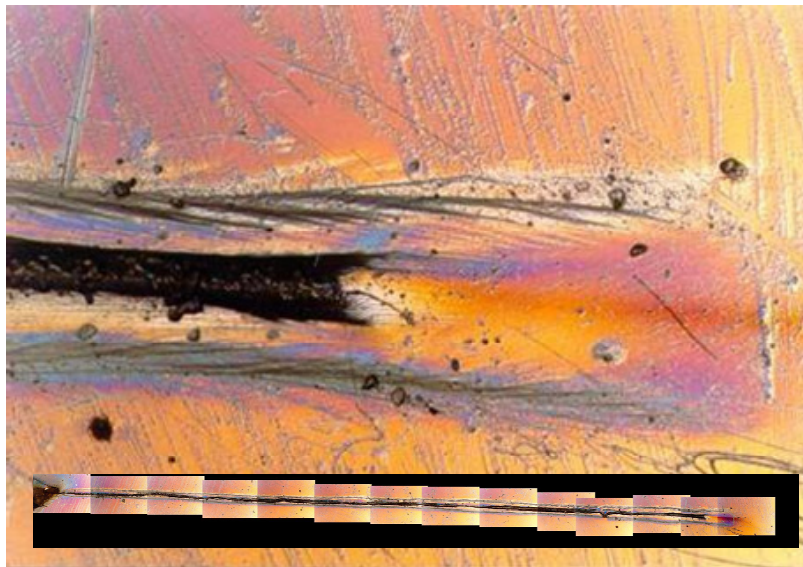


Figure 1: Mosaic of photoelastic image of a 20mm long fatigue crack in polycarbonate (inset) with the detail around the crack tip (main image) showing the presence of a process zone and a plastic wake.

## RESULTS AND DISCUSSION

Relatively little effort has been made at direct measurement or assessment of the crack tip plastic zone in the past. Earlier attempts using photoelasticity [20], moiré [21] and stereoimaging [22] lacked resolution. More recently techniques such as electronic speckle pattern interferometry [23], orientation gradient mapping and electronic channeling contrast imaging [24] have been used. Rajic et al [25] used the temperature of the plastic zone to define its extent in a similar way to the technique used to obtain the data in Fig. 2.

The use of photoelasticity, thermoelastic stress analysis and digital image correlation allows a more complete picture of the nature of plastic behaviour associated with fatigue crack growth to be constructed. The images in Fig. 1 show a Dugdale-type plastic zone with some variation in width as the crack extends. Shear bands are visible along the elastic-plastic boundary and help to define the extent of the plastic zone at the crack tip. Closer examination of the fringe patterns



reveals local strain raisers in the plastic zone as a result of plasticity-induced contact and fracture surface mismatch. It is interesting to note that the elastic material is largely shielded from these localised effects. Although the mechanism of crack propagation at the micro-scale is different in polycarbonate compared to metals it has been argued that this will not influence the meso-scale interaction between the crack tip and the surrounding plastic zone, or the plastic-elastic interactions [9]. Observation of this behaviour led the authors to consider the development of a new model of the forces acting on the elastic field surrounding the crack and its plastic enclave [26] which will be discussed in part 2 [1].

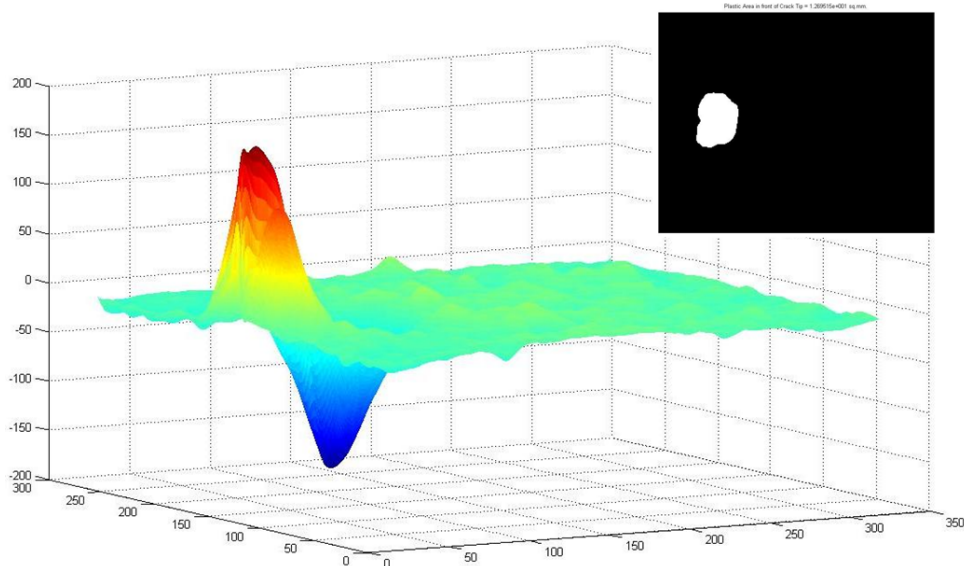


Figure 2: Map of the phase difference between the forcing signal (applied loading) and the measured temperature (due to the thermoelastic effect) and inset the result of applying a binary threshold to the data in order to identify the extent of the crack tip plastic zone.

It has been argued [12, 16] that heat generated by the plastic deformation during the application of load in the fatigue cycle causes the loss of adiabaticity ahead of the crack seen in Fig. 2. While frictional heating due to contact of the crack flanks during the unloading portion of the fatigue cycle causes the loss of adiabaticity observed behind the crack tip in Fig. 2. Since these two instances of heat generation occur in opposite parts of the loading cycle they would be expected to produce phase deviations of opposite sign as seen in Fig. 2. The actual sign of the phase difference is arbitrary and dependent on the set-up of the instrumentation. It is relatively straightforward to calculate the average diameter of the crack tip plastic zone based on a binary image obtained from the phase map. It is interesting, and perhaps re-assuring, to note that the resultant data lies mid-way between the estimates obtained using Dugdale's and Irwin's approximations, as seen in Fig. 4. Recently, Patki and Patterson [16] have used this approach to demonstrate the growth of the plastic zone during overloads that corresponds to a reduction in crack tip stress intensity factor and crack growth rate which all decay with cycles following the overload until the original or pre-overload magnitudes are achieved, as shown in Fig. 5. They went further and used the data to calculate the coefficients in Wheeler's empirical model [27] for overload behaviour and found good agreement with results from experiment.

The method employed to obtain the data in Fig. 3 builds on the approach employed by Lee et al [28] and Diaz et al [29] who used sub-image correlation of images of white light scattering from the surface of metallic specimens. In this case the distributions of maximum principal strains around a crack are shown for four crack lengths. The development of the shape and extent of the plastic zone with increasing crack length can be seen clearly. For one crack length ( $a=25.8\text{mm}$ ) the pitch of the displacement vectors was changed from  $0.038\text{mm}$  to  $0.113\text{mm}$  by changing the overlap of the facets from 2 pixels to 6 pixels. The effect of the increase in pitch is a reduction in spatial resolution of the displacement data and significant reduction in the quality of the strain map which emphasises the criticality of selecting appropriate processing parameters. The extent of the plastic zone was estimated from the strain values by assuming that strains greater than the material yield strain were plastic. This approach is potentially less reliable than thermoelastic method described above because it is dependent on a reliable material data and high-resolution digital image correlation data. However the estimates of the plastic zone size obtained from the dark red areas in Fig. 3 agree well with those calculated from Dugdale's model as shown in Fig. 4.

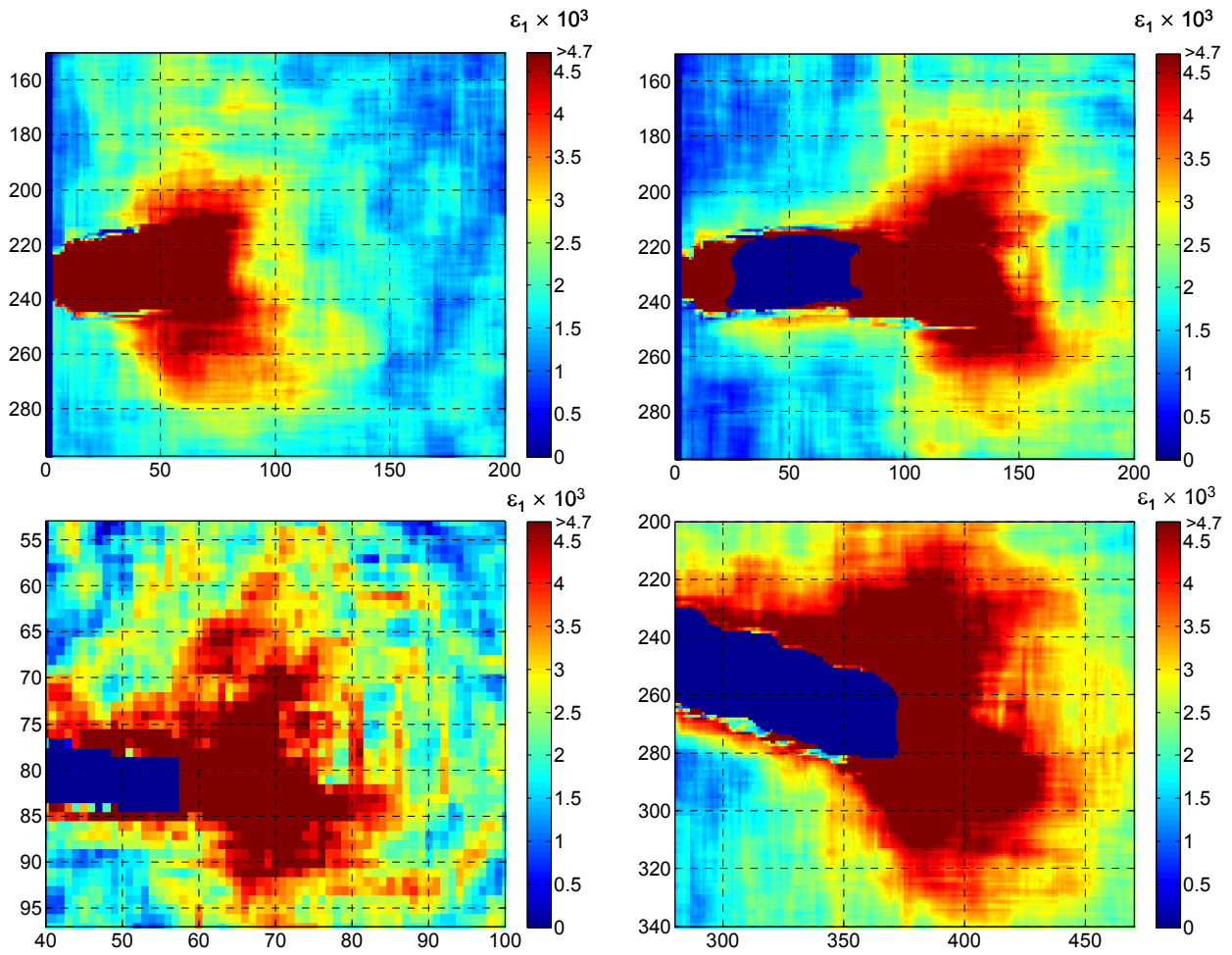


Figure 3: Distribution of maximum principal strain around the crack of length 21.2 (top left); 23.4 (top right); 25.8 (bottom left) and 32.8mm (bottom right) with strains above yield shown in dark red obtained using digital image correlation.

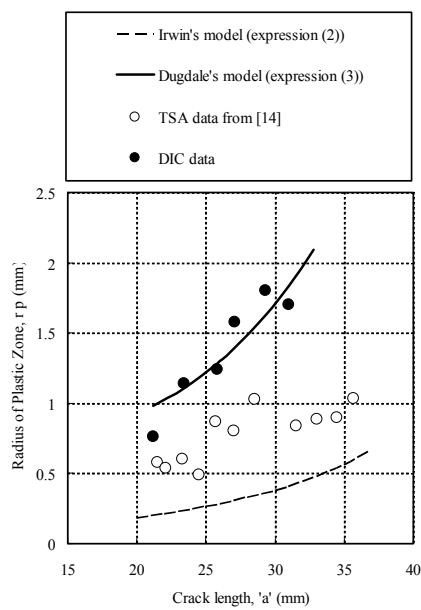


Figure 4: Plastic zone size as a function of crack length.

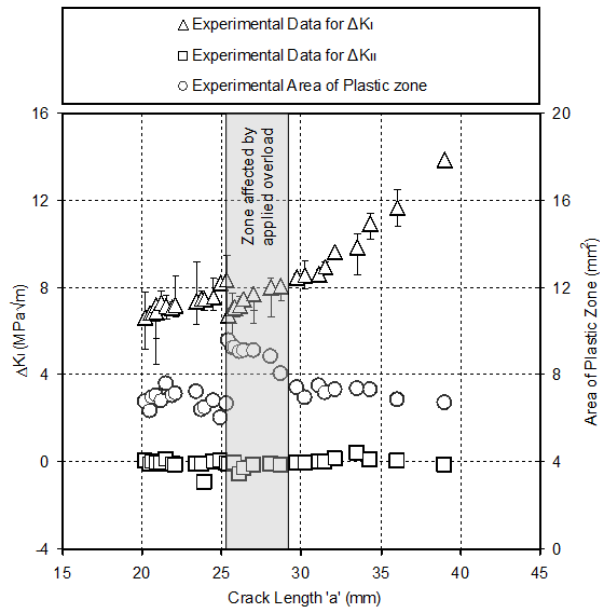


Figure 5: Stress intensity factors and plastic zone area as a function of crack length for a Al-alloy compact tension specimen subject to a 50% overload for ten cycles at a crack length of 25 mm (from [16]).

The shapes of the crack tip plastic zones in Figs. 1 to 3 are different and this is a reflection of the different approaches to their evaluation. The digital image correlation data are based on the maximum principal strain whereas the TSA and photoelastic data are based on the sum and difference, respectively of the principal strains. It should also be noted that the digital image correlation and TSA data were collected during the application of the fatigue load and that the digital image correlation data represents the maximum strain state whereas the TSA is based on behaviour throughout the cycle. However, photoelastic data has a very different basis since it was collected with no load applied to the specimen and hence the fringe pattern is representative of the residual strains induced by the fatigue crack growth process. The features seen in Fig. 1 led the authors to develop a schematic model of the forces acting at the interface between the plastic field or enclave surrounding the crack and the elastic field enclosing the plastic enclave [26, 30]. They, like others previously, surmised that the zone of plastically deformed material ahead of the crack would tend to induce a set of biaxial forces in the elastic field that in the unloaded state tend to compress the plastic enclave and which on loading needed to be overcome prior to any applied loading being experienced by the material at the crack tip. The portion of the plastic enclave found along the crack flanks is formed by the crack growth through the plastic zone ahead of the crack thus creating a plastic wake. The photoelastic fringe patterns suggest that a set of shear forces are established at the elastic-plastic interface in the wake which exist throughout the loading cycle but vary in magnitude and probably direction during the cycle. In addition, the authors assumed that in the unloaded state there were compressive forces acting perpendicular to the crack flanks on the plastic wake from the elastic region; and that these need to be overcome on loading before separation of the flanks occurs. These forces were added to the usual set of elastic forces assumed to be present in linear elastic fracture mechanics, including the forces due to the T-stress component, and used to develop a new multi-parameter model for the elastic stress system surrounding a crack. A schematic of the force system is shown in Fig. 6 and is developed in more detail in part 2 [1].

## CONCLUSIONS

The extent and shape of the plastic enclaves associated with fatigue crack growth have been obtained using three techniques from experimental mechanics, namely photoelasticity, thermoelastic stress analysis and digital image correlation. Quantitative data was obtained from two of the techniques during fatigue loading and showed reasonable agreement with models of crack tip plastic zone size developed by Dugdale and Irwin. These studies have inspired the development of new model of plasticity-induced shielding of the elastic strain field around a crack which helps to explain crack closure and the crack growth behaviour observed during overloads.

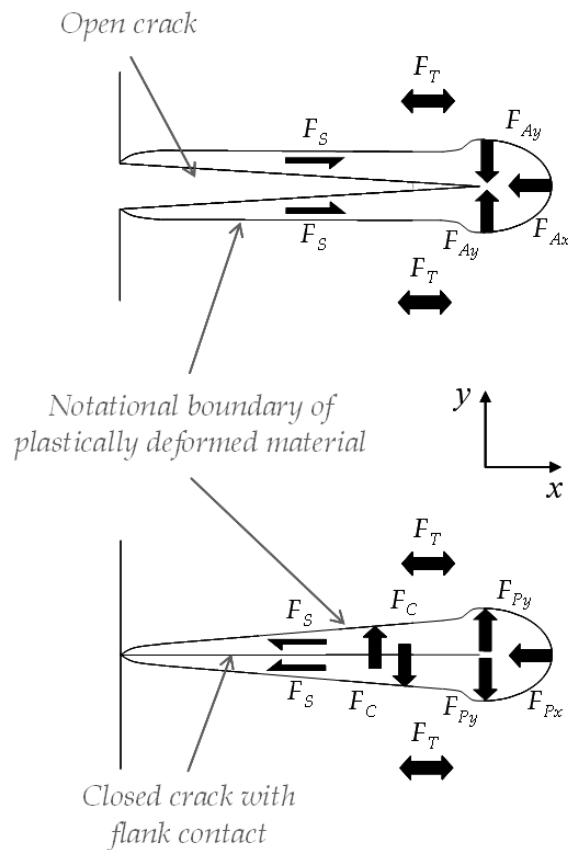


Figure 6: Schematic illustrating the forces acting on the elastic field surrounding the plastic zone around an open (*top*) and closed (*bottom*) crack. Equal and opposite forces will be acting on the plastic zone.  $F_A$  is the applied force generating the crack tip stress field characterized by  $K_I$ ;  $F_T$  is the force generated by the  $T$ -stress;  $F_S$  is the interfacial shear force at the elastic-plastic boundary;  $F_P$  is the force generated by the constraint of compatibility on the plastically deformed material and  $F_C$  is the contact force between the flanks of the crack arising from the interference of the plastic wakes (from [29]).

## REFERENCES

- [1] M. N. James, C. J. Christopher, Yanwei Lu, E. A. Patterson, In: Proc. Int. Conf. on Characterising Crack Tip Stresses, Forni di Sopra, UD, Italy, 7-9 March 2011.
- [2] W. Elber, Engng Fract Mech, 2(1970) 37.
- [3] M.N. James, In: Proc. 9<sup>th</sup> Int. Conf. on Fracture, Edited by. B.L. Karihaloo et al., Pergamon Press, 5 (1997) 2403.
- [4] N. Walker, C.J. Beevers, Fatigue Fract. Engng. Mater. Structs., 1 (1979) 135.
- [5] S. Suresh, G.F. Zamiski, R.O. Ritchie, Metall. Trans. A: Phys. Metall. & Mater. Sci., 12A (1981) 1435.
- [6] K. Endo, T. Okada, K. Komai, M. Kiyoto, Bull. JSME., 15 (1972) 1316.
- [7] A. G. Pineau, R. M. Pelloux, Metall. Trans., 5 (1974) 1103.
- [8] E. A. Patterson, In: Encyclopedia of Materials: Science and Technology, edited by K.H.J. Bushow, R.W. Cahn, M.C. Flemings, B. Ilshner, E.J. Kramer, S. Mahajan, P. Veysière, Elsevier Ltd., (2007) 6923.
- [9] M.N. Pacey, M.N. James, E.A. Patterson, Exptl. Mech., 45 (2005) 42.
- [10] R.J. Greene, E.A. Patterson, R.E. Rowlands, In: Handbook of Experimental Mechanics edited by W.N. Sharpe Jr., Springer, New York (2008).
- [11] G. Pitarresi, E.A. Patterson, J. Strain Analysis, 38 (2003) 405.
- [12] E.A. Patterson, F.A. Diaz, J.R. Yates, J. Testing & Evaluation, 3 (2006) paper id JAI13222.
- [13] M.A. Sutton, J.-J. Orteu, H.W. Schreier, Image Correlation for Shape, Motion and Deformation Measurements, Springer, New York, (2009).
- [14] P. Lopez-Crespo, A. Shterenlikht, E.A. Patterson, P.J. Withers, J.R. Yates, J. Strain Analysis, 43 (2008) 769.



- [15] M.N. James, M.N. Pacey, L-W. Wei, E.A. Patterson, E.A., *Engineering Fracture Mechanics*, 70 (2003) 2473.
- [16] A. S. Patki, E.A. Patterson, *Fatigue and Fracture of Engineering Materials and Structures*, 33 (2010) 809.
- [17] Y. Du, A.S. Patki, E.A. Patterson, In: *Proc. 2010 SEM Conf. Exptl. & Appl. Mech.*, Indianapolis, IN, (2010) paper #270.
- [18] D.S. Dugdale, *J. Mechs. & Phys. Solids*, 8 (1960) 100.
- [19] G.R. Irwin, *Engng. Fract. Mechs.*, 1 (1968) 241.
- [20] W.W. Gerberich, J.L. Swedlow, *Experimental Mechanics*, 4 (1964) 345.
- [21] H.W. Liu, N. Lino, N., *Fracture 1969, Proc. 2<sup>nd</sup> Int. Conf.*, England, (1969) 812.
- [22] D.R. Williams, D.L. Davidson, J. Lankford, *Experimental Mechanics*, 20 (1980) 134.
- [23] K-S. Kim, K-S. Kim, C-S. Shim, *Structural Engineering and Mechanics*, 15 (2003) 367.
- [24] M.T. Welsch, M. Henning, M. Marx, H. Vehoff, *Advanced Engineering Materials*, 9 (2007) 31.
- [25] N. Rajic, Y.C. Lam, A.K. Wang, *Trans. ASME. J. Engng. Materials and Technology*, 119 (1997) 32.
- [26] C.J. Christopher, M.N. James, E.A. Patterson, K.F. Tee, *IJ Fracture*, 148 (2007) 361.
- [27] O.E. Wheeler, *Journal of Basic Engineering*, D94 (1972) 181.
- [28] C. Lee, Y.J. Chao, M.A. Sutton, W.H. Peters, W.F Ranson, *Experimental Mechanics*, 29 (1989) 214.
- [29] F.V. Diaz, G.H. Kaufmann, A.F. Armas, G.E. Galizzi, *Optics and Lasers in Engineering*, 35 (2001) 325.
- [30] C.J. Christopher, M.N. James, E.A. Patterson, E.A., K.F. Tee, *Engng. Fract. Mechanics*, 75 (2008) 4190.